Ru et al. *Zool. Res.* 2025, 46(5): 1187−1202
https://doi.org/10.24272/j.issn.2095-8137.2025.211
https://cstr.cn/32248.14.zr.2025.211

ZR | Zoological Research

Article Open Access

Ultra-short cyclic peptide $Cy_{RL-QN15}$ acts as a TLR4 antagonist to expedite oral ulcer healing

Ze-Qiong Ru[1,#], Yu-Tong Wu[2,#], Chong-Yu Yang[1,#], Ya-Ting Yang[1], Ya-Jie Li[1], Min Liu[1], Ying Peng[1], Yu-Liu Yang[1], Jun-Yuan Wang[3], Qiu-Ye Jia[1], Yuan-Sheng Li[1], Zhe Fu[1], Mei-Feng Yang[1], Jing Tang[2], Yan Fan[1], Cheng-Xing Liu[1], Wen-Rou Su[4], Nai-Xin Liu[1,*], Li He[5,*], Ying Wang[3,*], Xin-Wang Yang[1,4,*]

[1] *Department of Anatomy and Histology & Embryology*, *Faculty of Basic Medical Science*, *Kunming Medical University*, *Kunming*, *Yunnan* 650500, *China*

[2] *Department of Biochemistry and Molecular Biology*, *Faculty of Basic Medical Science*, *Kunming Medical University*, *Kunming*, *Yunnan* 650500, *China*

[3] *Key Laboratory of Chemistry in Ethnic Medicinal Resources & Key Laboratory of Natural Products Synthetic Biology of Ethnic Medicinal Endophytes*, *State Ethnic Affairs Commission & Ministry of Education*, *School of Ethnic Medicine*, *Yunnan MinZu University*, *Kunming*, *Yunnan* 650504, *China*

[4] *Yunnan Yunke Characteristic Plant Extraction Laboratory Co., Ltd.*, *Kunming*, *Yunnan* 650106, *China*

[5] *Department of Dermatology*, *First Affiliated Hospital of Kunming Medical University*, *Kunming*, *Yunnan* 650032, *China*

ABSTRACT

Oral ulcers (OUs) are among the most common lesions of the oral mucosa, typically associated with pain and burning sensations, and remain clinically challenging due to the scarcity of effective treatment options. $Cy_{RL-QN15}$, a novel ultra-short cyclic heptapeptide recently shown to promote skin repair, diabetic wound healing, and follicle neogenesis, was evaluated for its therapeutic potential in mucosal repair. Using a rat OU model and a primary oral epithelial cell inflammation model, $Cy_{RL-QN15}$ significantly accelerated wound closure through coordinated modulation of immune-epithelial crosstalk, including suppression of inflammatory cytokine release from macrophages and neutrophils, reduction of pro-inflammatory factor secretion by oral epithelial cells, and enhancement of their proliferation and migration. Mechanistic studies employing alanine scanning mutagenesis and microscale thermophoresis revealed that $Cy_{RL-QN15}$ directly interacted with Toll-like receptor 4 (TLR4) via a methionine-dependent binding interface (K_d=2.64 μmol/L), thereby inhibiting downstream MyD88/NF-κB signaling. As the first ultra-short cyclic heptapeptide identified to antagonize TLR4, $Cy_{RL-QN15}$ represents a mechanistically distinct immunomodulatory scaffold that restores mucosal homeostasis and offers a promising therapeutic candidate for TLR4-based OU intervention.

Keywords: Ultra-short peptide; Oral ulcer; TLR4 antagonist; Inflammation; MyD88/NF-κB signaling pathway; Macrophage polarization

INTRODUCTION

The oral mucosa serves as a crucial barrier at the interface of the digestive and respiratory tracts, providing frontline protection against mechanical injury, environmental toxins, and microbial invasion (Şenel, 2021; Waasdorp et al., 2021). Oral ulcers (OUs), which affect approximately 5%–25% of the global population, represent one of the most prevalent pathologies of the oral mucosa and are frequently associated with considerable pain, dysphagia, speech impairment, and psychological distress, imposing a substantial burden on both individuals and the healthcare system (Ślebioda et al., 2014; Shi et al., 2021). While most OUs resolve spontaneously, recurrent or persistent lesions often result in significant morbidity.

Received: 05 July 2025; Accepted: 29 August 2025; Online: 30 August 2025

Foundation items: This work was supported by the National Natural Science Foundation of China (32301054, 82404582, 32360138, 32060212), First-Class Discipline Team of Skin & Mucosal Regenerative Medicine of Kunming Medical University (2024XKTDTS10), Key Program of Yunnan Fundamental Research Project (202301AS070036), Open Research Fund of Yunnan Characteristic Plant Extraction Laboratory (YKKF2024003), and Project of Yunnan Applied Basic Research Project-Kunming Medical University Union Foundation (202301AY070001-301, 202401AY070001-028, 202301AY070001-012, 202401AY070001-068, 202301AY070001-169)

[#]Authors contributed equally to this work

*Corresponding authors, E-mail: liunaixin@kmmu.edu.cn; drheli2662@126.com; wangying_814@163.com; yangxinwang@kmmu.edu.cn

The pathogenesis of OU involves a multifactorial network of genetic susceptibility, immune dysregulation, and environmental triggers, including autoimmune conditions and psychological stress (Al-Omiri et al., 2015; Dudding et al., 2019). Despite growing insights into the contributing factors, the underlying etiology remains poorly understood, hindering the development of targeted therapeutic interventions. Current treatments may offer symptomatic relief but are limited by adverse effects. For instance, corticosteroids, such as triamcinolone, may compromise host immune responses; nonsteroidal anti-inflammatory drugs (NSAIDs) increase the risk of gastrointestinal bleeding; and chlorhexidine (CHX, 0.2% w/v) can cause enamel staining and dysgeusia (Addy, 1977; Wu et al., 2009). These limitations underscore an urgent need for innovative therapeutic agents capable of restoring mucosal integrity while minimizing systemic toxicity.

The healing cascade proceeds through a tightly regulated sequence of overlapping stages, including hemostasis, inflammation, proliferation, and remodeling, each orchestrated by a dynamic interplay of cellular and molecular events (Joorabloo & Liu, 2024; Toma et al., 2021; Waasdorp et al., 2021). A critical regulatory checkpoint lies in the inflammatory-to-proliferative phase transition, which is governed by cytokine levels and the inflammatory response. Dysregulation in this transition can prolong inflammation, increase susceptibility to infection, impair re-epithelialization, and trigger tissue necrosis. Thus, maintaining balanced progression through these phases is essential for efficient tissue repair (Landén et al., 2016; Li et al., 2024b). During the early inflammatory stage, macrophages initiate cytokine-mediated immune responses—secreting interleukin-1 (IL-1) and tumor necrosis factor-alpha (TNF-α)—and facilitate the recruitment of oral epithelial cells to the wound site. As healing progresses, macrophages undergo a phenotypic shift from pro-inflammatory M1 to pro-resolving M2 polarization, enhancing interleukin-10 (IL-10) secretion to suppress excessive inflammation and accelerate transition to the proliferative phase (Toma et al., 2021; Wu et al., 2022). Preservation of oral epithelial integrity is indispensable for mucosal homeostasis, with epithelial cells serving as the primary barrier against microbial invasion. Impaired proliferative capacity in these cells compromises epithelial tight junctions, facilitating microbial penetration and worsening OU pathology (Wu et al., 2010). As a crucial bridge between innate and adaptive immunity, Toll-like receptor 4 (TLR4), a type I transmembrane pattern recognition receptor highly expressed in the oral epithelium (Darveau & Curtis, 2021; Groeger & Meyle, 2019; Lukova et al., 2020), plays a central role in the regulation of innate and adaptive immune signaling. TLR4 regulates inflammatory processes within the oral mucosa via the MyD88/NF-κB signaling pathway (Jin et al., 2022; Shi et al., 2022; Wang et al., 2021a) and contributes to the immunopathology of chronic inflammation. Aberrant polarization of TLR4 observed in ulcerated mucosa (Hietanen et al., 2012) reflects persistent inflammatory activation and highlights its essential role in maintaining immune homeostasis. Notably, excessive TLR4 activation has been mechanistically linked to the pathogenesis of various autoimmune diseases, including rheumatoid arthritis and systemic lupus erythematosus (Li et al., 2022b; Liu et al., 2024b; Summers et al., 2010). These findings implicate TLR4 as a promising therapeutic target whose inhibition may promote inflammation-to-proliferation conversion and restore immune equilibrium, offering a novel strategy for the treatment of autoimmune-related oral ulceration.

Bioactive peptides derived from amphibians, such as RL-QN15, cathelicidin-OA1, and Andersonin-W1, have garnered significant interest due to their potent therapeutic properties (Cao et al., 2018; Li et al., 2024a; Sun et al., 2021, 2023; Wang et al., 2021b). Among these, cyclic peptides are recognized for their exceptional stability, high specificity, strong binding affinity, and multifunctionality (Gang et al., 2018; Ji et al., 2024). Ultra-short peptides, typically comprising no more than seven amino acids, offer additional advantages such as cost-effectiveness, ease of synthesis, enhanced stability, and low immunogenicity (Ni, 2019; Seow & Hauser, 2014). Despite their therapeutic potential, research on peptide-based TLR4 antagonists remains relatively limited. Owing to their compact structure, minimal off-target activity, and innate biocompatibility, ultra-short cyclic peptides constitute an ideal scaffold for the development of targeted and innovative OU therapies (Levin et al., 2020; Li et al., 2024d; Zhang et al., 2022b).

This study investigated the therapeutic potential of $Cy_{RL\text{-}QN15}$, an ultra-short cyclic peptide composed of seven amino acids arranged in a ring structure. Previous research has demonstrated that $Cy_{RL\text{-}QN15}$ accelerates dermal repair, promotes hair follicle neogenesis, and enhances diabetic wound healing in preclinical models (Jia et al., 2024; Wu et al., 2024). Given the parallels between OU healing and skin wound repair, we hypothesized that bioactive peptides known to enhance skin wound healing may induce similar pro-healing effects on OUs. Notably, results showed that $Cy_{RL\text{-}QN15}$ exerted an antagonistic effect by directly binding to TLR4 receptors, inhibiting the downstream MyD88/NF-κB pathway, and triggering inflammatory-to-proliferative phase transition, ultimately contributing to OU recovery. These data establish $Cy_{RL\text{-}QN15}$ as a novel TLR4 antagonist capable of modulating immune-epithelial crosstalk to restore mucosal integrity, highlighting its translational potential as a next-generation biotherapeutic for oral ulcer management.

MATERIALS AND METHODS

Ethics approval and consent to participate

All procedures related to animal care and handling were approved by the Ethics Committee of Kunming Medical University (approval no. kmmu20240246) and conducted in accordance with its guidelines. All experiments were performed in accordance with the Declaration of Helsinki.

Peptide synthesis

$Cy_{RL\text{-}QN15}$ (CQFHYMC), FITC-labeled $Cy_{RL\text{-}QN15}$, and its mutants (CYM1: CQFAYMC, CYM2: CQFHAMC, and CYM3: CQFHYAC), with purities exceeding 95%, were commercially synthesized by Wuhan Tanda Biotechnology (China). All peptides were prepared via Merrifield solid-phase peptide synthesis (SPPS), proceeding from the C-terminus to N-terminus. Synthesis commenced with covalent attachment of the C-terminal amino acid to an insoluble polymer resin. Each cycle comprised amine deprotection of the resin-bound residue, followed by stepwise coupling of the next amino acid through activation of its carboxyl group, thereby forming successive amide bonds and extending the peptide chain. The iterative synthesis cycle included: (1) condensation, (2) resin washing to remove unreacted reagents, (3) amine deprotection, (4) neutralization to prepare the amine group for subsequent coupling, and (5) repetition of the cycle until the target peptide length was achieved. Final products were cleaved from the

resin, purified, and lyophilized. Identity and purity were confirmed by high-performance liquid chromatography (HPLC) (Supplementary Figure S1) and mass spectrometry (MS) (Supplementary Figure S2). Detailed physicochemical properties of the peptides are provided in Supplementary Figure S3 and Supplementary Table S1.

Animal ethics statement and informed consent

Male Sprague-Dawley (SD) rats (180–220 g, 8–10 weeks old) were obtained from Hunan SJA Laboratory Animal Co., Ltd. (China) and maintained in a pathogen-free facility under a 12-h light/dark cycle. All animal-related experimental procedures were reviewed and approved by the Ethics Committee of Kunming Medical University (approval no. kmmu20240246), in strict accordance with the institution's ethical guidelines. All experimental procedures were conducted in a blinded manner, and no outliers were excluded from analysis.

Establishment and treatment of OU model

The OU model was established by acid-induced gingival injury, as described previously (Ayoub et al., 2022; El-Zahar et al., 2022; Hitomi et al., 2016). Rats were anesthetized via intraperitoneal (IP) injection of ketamine (40 mg/kg) and xylazine (5 mg/kg), followed by placement of a 3 mm filter paper disc pre-soaked in 50% acetic acid solution on the mandibular gingiva for 1 min. After acid exposure, rats were fasted for 30 min without access to food or water and allowed to recover beside a temperature-controlled heater. By postoperative day 2, formation of a well-defined 3 mm-diameter OU was confirmed and designated as experimental day 0. Rats were then randomly assigned to three groups: Vehicle (phosphate-buffered saline (PBS) control), CHX (0.2% w/v, positive control), and $Cy_{RL\text{-}QN15}$ (100 nmol/L). Treatments were administered directly to the wound area twice daily (50 μL per dose) (da Silveira Teixeira et al., 2019). OU wounds were monitored and photographed on days 0, 3, 6, and 8, with sampling performed on days 3 and 8 post-treatment. Changes in the OU area and oral epithelium thickness were assessed using ImageJ software.

Hematoxylin and eosin (H&E) staining

Oral mucosal tissues were collected on days 3 and 8 post-treatment for histological evaluation. Samples were embedded in medium within plastic cassettes, and 8 μm frozen sections were prepared. H&E staining was performed to assess epithelial regeneration and basement membrane architecture, followed by microscopic examination (Zeiss, Germany) (Zhang et al., 2023b).

Immunohistochemical (IHC) staining

Frozen tissue sections were fixed for 10 min and incubated with blocking buffer at room temperature for 30 min. The sections were then incubated at 37°C for 1 h with primary antibodies, including rabbit anti-myeloperoxidase (anti-MPO) (Wanlei Bio, China) and anti-inducible nitric oxide synthase (anti-iNOS) (Wanlei Bio, China), followed by chromogenic detection with 3,3'-diaminobenzidine (DAB, ZSGB Bio, China). Positively stained cells were quantified and analyzed under a microscope (Zeiss, Germany).

Tissue 5-ethynyl-2'-deoxyuridine (EdU) staining

Cell proliferation in oral mucosal tissue was assessed using an EdU detection kit (Beyotime, China). On days 3 and 8 post-treatment, EdU (20 mg/kg) was administered to SD rats via IP injection. After 4 h, tissue samples were harvested and counterstained with 4',6-diamidino-2-phenylindole (DAPI). EdU-positive cells were visualized and quantified using a laser scanning confocal microscope (Nikon, Japan) (Wang et al., 2023).

Immunofluorescence (IF) staining

Oral mucosal tissue sections were washed in PBS, equilibrated to room temperature, and blocked for 1 h in a solution containing 0.3% Triton X-100 and 5% goat serum. Cryosections were then incubated overnight at 4°C with primary antibodies against TNF-α (Proteintech, USA), IL-1β (Proteintech, USA), and IL-10 (Affinity, China). After washing, the sections were then incubated with secondary antibodies (Cy3, Proteintech, USA; ABflo488, ABclonal, China) for 1 h at 37°C. Nuclei were counterstained with DAPI, and fluorescence images were captured and analyzed using a laser scanning confocal microscope (Nikon, Japan).

Oral mucosa permeability of $Cy_{RL\text{-}QN15}$

FITC-labeled $Cy_{RL\text{-}QN15}$ (100 nmol/L) was topically applied to the lower gingiva of SD rats. Oral mucosal tissue was collected at 0.5, 1, 2, and 4 h post-application, embedded in optimal cutting temperature (OCT) compound, and cryosectioned at a thickness of 8 μm. Images were captured using a laser scanning confocal microscope (Nikon, Japan) in a dark room to assess $Cy_{RL\text{-}QN15}$ permeability through the oral mucosa.

Primary oral epithelial cell extraction

Primary oral epithelial cells were isolated from the oral mucosa of SD rats using previously described protocols (Hu et al., 2023; Rakhorst et al., 2006; Xie et al., 2021). Briefly, oral mucosal tissue was collected under sterile conditions and incubated in dispase II (2.5 mg/mL, Coolaber, China) at 4°C for 16 h. The oral epithelial layer was then separated using sterile forceps and incubated in a mixture of collagenase Ⅰ(2 mg/mL, Solarbio, China) and hyaluronidase (1 mg/mL, Solarbio, China) at 37°C for 4 h. The digestion solution was strained over a 70 μm mesh filter. Primary oral epithelial cells were obtained by centrifugation at 400 ×*g* for 5 min at room temperature.

Cell culture

Primary oral epithelial cells were cultured in Dulbecco's Modified Eagle Medium/Nutrient Mixture F-12 (DMEM/F12; BI, Israel) supplemented with 10% fetal bovine serum (FBS, HyClone, USA) and 1% antibiotics (penicillin, streptomycin, and amphotericin B, Absin, China). Upon reaching 80% confluence at the third passage, cells were seeded at a density of 1×10^5 cells/well in a 24-well plate. Prior to inflammatory stimulation, cells were pretreated with $Cy_{RL\text{-}QN15}$ (100 nmol/L) for 6 h. Lipopolysaccharide (LPS, 2 μg/mL, Sigma, USA) was then added, and cells were incubated for 24 h to establish an inflammatory model.

Cell proliferation

Cell proliferation was assessed using the CCK-8 assay kit (Dojindo, Japan) to evaluate the effects of $Cy_{RL\text{-}QN15}$ and TLR4 inhibitors (TAK242, 1 μmol/L, MCE, USA) on oral epithelial cell proliferation. Third-generation oral epithelial cells, cultured to 80% confluence, were seeded in 96-well plates at a density of 6 000 cells/well. After cell adhesion, TLR4 inhibitors and $Cy_{RL\text{-}QN15}$ were added sequentially. Following 12 h of incubation at 37°C, CCK-8 solution was added and incubated for 1.5 h. Absorbance at 450 nm was then measured using a microplate reader (SpectraMax 190, USA) (Cha et al., 2024; Wang et al., 2025).

Cell migration

Cell migration was assessed using Transwell chambers (8 μm pore size, Corning, USA). Third-passage oral epithelial cells were seeded in T25 flasks and grown to 80% confluence before seeding in Transwell chambers at a density of 1×10^5 cells. The cells were then assigned to four groups: control, $Cy_{RL\text{-}QN15}$ (1 nmol/L), $Cy_{RL\text{-}QN15}$ (10 nmol/L), and $Cy_{RL\text{-}QN15}$ (100 nmol/L). After 24 h, the cells were stained with crystal violet (0.5 mg/mL) for 20 min. Excess stain was softly wiped off the surface of the filter membrane. Absorbance at 570 nm was observed to evaluate the impact of varying concentrations of $Cy_{RL\text{-}QN15}$ on the migratory capacity of oral epithelial cells (Zhang et al., 2022).

Western blot analysis

Total protein was extracted from oral mucosal tissue and concentrations were determined using a BCA protein assay kit (Beyotime, China). Samples were denatured by heating at 95°C for 15 min. Protein expression in the OU rat model was assessed using western blotting, with β-tubulin serving as an internal control. Proteins were resolved by sodium dodecyl sulfate-polyacrylamide gel electrophoresis (SDS-PAGE), transferred to polyvinylidene fluoride (PVDF) membranes, and blocked with a protein-free rapid blocking solution (Epizyme, China) for 5 min. The membranes were then incubated at 4°C overnight with primary antibodies against MyD88 (Affinity, China), IκB (Affinity, China), P-IκB (Affinity, China), P65 (Affinity, China), P-P65 (Affinity, China), and β-tubulin (Affinity, China). After three washes, the membranes were incubated for 1 h at 37°C with secondary antibodies (Affinity, China). Protein bands were detected using a chemiluminescence substrate (Biosharp, China) and imaged on a chemiluminescence imaging system. Gray values of protein bands were evaluated using ImageJ software (Liu et al., 2020).

Reverse transcription-quantitative real-time polymerase chain reaction (RT-qPCR)

Total RNA was isolated using a commercial RNA extraction kit (Agbio, China). Quantitative amplification of target genes was performed using an Evo M-MLV One-Step RT-qPCR kit (Agbio, China), with *GAPDH* as the internal reference. Gene expression was quantified relative to the control using the comparative Ct method. All primers used are listed in Supplementary Table S2 (Jin et al., 2022).

mRNA sequencing

SD rats were randomly allocated to Vehicle and $Cy_{RL\text{-}QN15}$ treatment groups based on previously described protocols (Ayoub et al., 2022; El-Zahar et al., 2022; Fujisawa et al., 2003; Hitomi et al., 2016). Oral mucosal tissues were collected on day 3 post-treatment and sent to Major Biotechnology for RNA sequencing. Differentially expressed genes (DEGs) were identified based on a threshold of $P<0.05$ and fold change> 2. Gene Ontology (GO) enrichment analysis was conducted across biological process (BP), cellular component (CC), and molecular function (MF) categories. Kyoto Encyclopedia of Genes and Genomes (KEGG) enrichment analysis was performed to identify significantly enriched signaling pathways, highlighting the potential healing properties of $Cy_{RL\text{-}QN15}$.

Molecular docking

Molecular docking was employed to explore the interaction between $Cy_{RL\text{-}QN15}$ and TLR4 (An et al., 2021). The three-dimensional (3D) structure of rat TLR4 (ID: Q9QX05), serving as the receptor protein (R), was obtained from AlphaFold. The structure of $Cy_{RL\text{-}QN15}$, acting as the ligand (L), was modeled using PyMOL. Molecular docking was carried out using the Z-Dock server (https://zdock.umassmed.edu/), with the highest-scoring conformations selected for subsequent molecular dynamics simulations to refine binding interactions and improve docking accuracy.

Microscale thermophoresis (MST) assay

MST analysis was performed using a Monolith NT.115 instrument (NanoTemper Technologies, Germany). Purified recombinant TLR4 protein (>97% purity; 12.5 nmol/L; Cloud Clone, China) was fluorescently labeled using a RED-Tris-NTA labeling kit (NanoTemper, Germany). $Cy_{RL\text{-}QN15}$ and its mutants (CYM1, CYM2, and CYM3) were serially diluted in 15 steps from an initial concentration of 500 μmol/L. Equal volumes of labeled TLR4 and peptide solutions were mixed in reaction buffer (20 mM HEPES, pH 7.0, 150 mmol/L NaCl, 0.02% (w/v) DDM) and loaded into capillaries. Measurements were conducted under 40% LED excitation power and medium MST power. Data were analyzed using NanoTemper software (v2.3) (Li et al., 2019).

Statistical analysis

Statistical analyses were performed using GraphPad Prism v.7 (GraphPad Software Inc., USA). Data are presented as mean±standard error of the mean (SEM), with $P<0.05$ considered statistically significant. One-way or two-way analysis of variance (ANOVA) followed by Tukey's *post-hoc* test was used for comparisons among different groups.

RESULTS

$Cy_{RL\text{-}QN15}$ promotes OU healing in SD rats

An acid-etching method was used to establish a chemically induced OU model in the gingival tissue of SD rats. Wound progression was monitored on days 0, 3, 6, and 8 (Figure 1A, B). By day 3, the $Cy_{RL\text{-}QN15}$ treatment group exhibited a mean healing rate of approximately 75%, markedly higher than that of the Vehicle group (42%) and comparable to the CHX group (72%) (Figure 1C). By day 8, both $Cy_{RL\text{-}QN15}$ and CHX groups showed near-complete wound closure, while the Vehicle group reached only 81% healing. Notably, the $Cy_{RL\text{-}QN15}$ group (100 nmol/L) achieved therapeutic efficacy comparable to that of CHX (2 mmol/L), despite the substantially lower nanomolar concentrations, indicating potent regenerative capacity. Histological assessment via H&E staining confirmed these findings. On day 3, all groups exhibited substantial epithelial disruption, loss of basement membrane integrity, and inflammatory cell infiltration at the ulcer margin (Figure 1D). By day 8, epithelial regeneration and basement membrane reconstitution were evident in both $Cy_{RL\text{-}QN15}$ and CHX groups, with wound closure approaching 100%, whereas the Vehicle group achieved only 81%. $Cy_{RL\text{-}QN15}$ treatment yielded a 1.23-fold improvement in wound closure compared to the Vehicle control. Notably, epithelial thickness in the $Cy_{RL\text{-}QN15}$ group was 1.43-fold greater than in the Vehicle group, indicating a significant enhancement in mucosal regeneration (Figure 1E). To evaluate tissue permeability, FITC-labeled $Cy_{RL\text{-}QN15}$ was visualized by immunofluorescence. Progressive peptide penetration was observed from the epithelial layer into the basement membrane and deeper submucosal layers (Figure 1F), demonstrating that $Cy_{RL\text{-}QN15}$ effectively traverses the oral mucosa to access target tissue compartments.

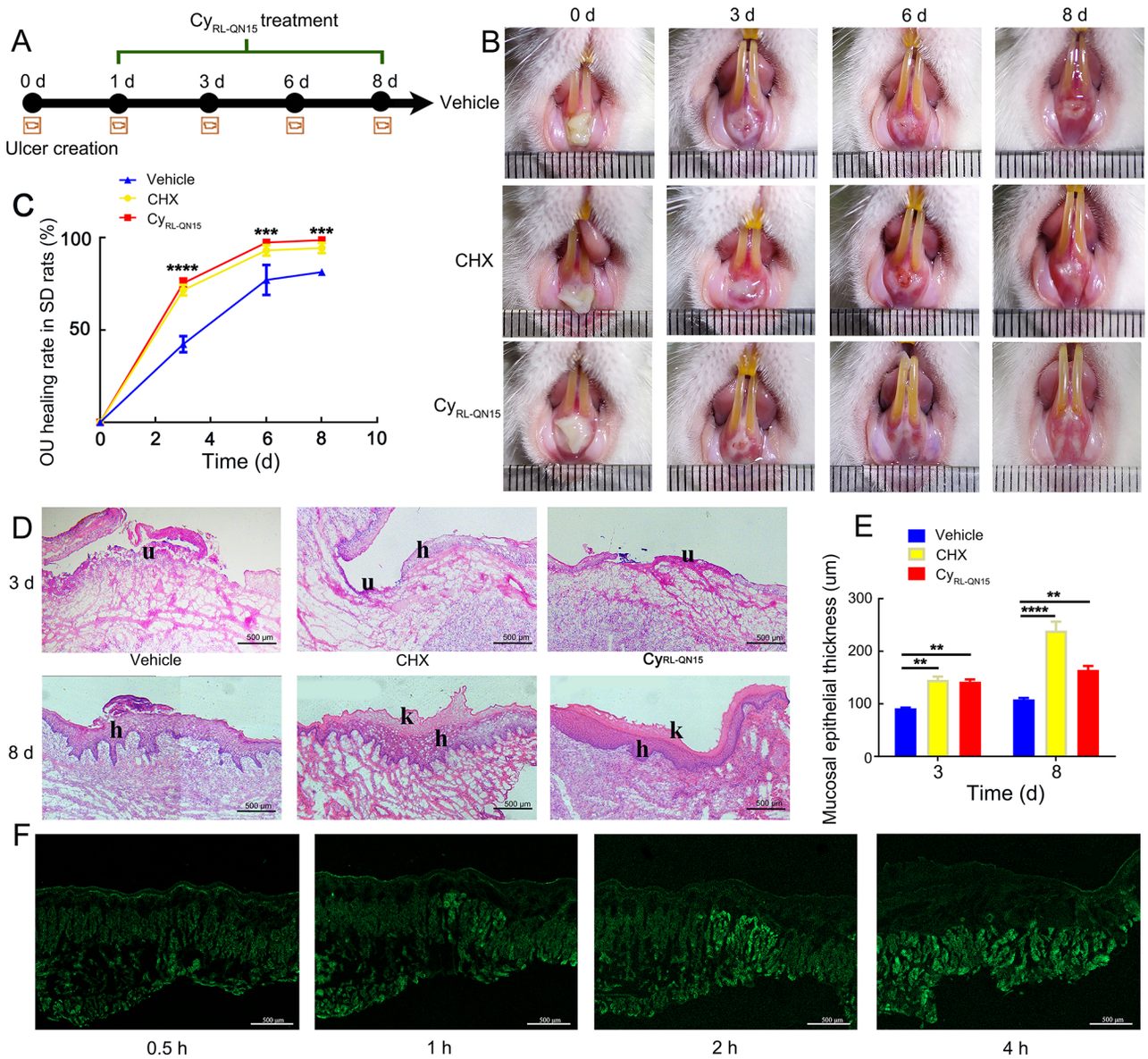

Figure 1 Local application of Cy$_{RL-QN15}$ accelerates healing of acid-induced OU in SD rats

A: Schematic of acid-induced OU and Cy$_{RL-QN15}$ treatment protocols. B: Representative images of OU healing progress (days 0, 3, 6, and 8) in Vehicle, CHX, and Cy$_{RL-QN15}$ groups. C: Quantitative analysis of OU healing rate in SD rats (n=5). D: Representative H&E-stained images of OU sites (days 3 and 8). u: Ulcerated oral epithelium; h: Hyperplastic epithelium; k: Hyperkeratosis. Scale bar: 500 μm. E: Quantification of mucosal epithelial thickness (basement membrane to stratum corneum) (n=5). F: Tissue permeability of FITC-labeled Cy$_{RL-QN15}$ (green) in oral mucosa. Scale bar: 500 μm (n=4). All data are presented as mean±SEM. **: P<0.01; ***: P<0.001; ****: P<0.0001. Data analyzed by one-way ANOVA with Tukey's multiple comparisons test.

Cy$_{RL-QN15}$ modulates cytokine release from macrophages and neutrophils

The inflammatory phase plays a critical role in coordinating mucosal repair, with macrophages serving as key immune modulators (Li et al., 2022a; Sharifiaghdam et al., 2022). IL-1β and TNF-α are canonical markers of pro-inflammatory M1 macrophages, while IL-10 is indicative of anti-inflammatory M2 macrophages. Furthermore, inducible nitric oxide synthase (iNOS) is a well-established functional marker of M1 macrophages. Immunofluorescence staining on days 3 and 8 revealed that Cy$_{RL-QN15}$ significantly down-regulated IL-1β and TNF-α expression while up-regulating IL-10 expression, indicating a shift toward a pro-resolving immune phenotype (Figure 2A–D). Complementary immunohistochemical analysis confirmed significantly reduced iNOS expression in Cy$_{RL-QN15}$-treated tissue compared with the Vehicle control (Figure 2E–G), indicating a shift toward an anti-inflammatory microenvironment in the mucosal wound area. Myeloperoxidase (MPO), a neutrophil-associated enzyme, was also significantly down-regulated by day 8 following Cy$_{RL-QN15}$ treatment, as shown by IHC staining. These findings suggest that Cy$_{RL-QN15}$ promotes mucosal healing by modulating macrophage polarization and suppressing neutrophil-driven inflammation within the ulcer microenvironment.

Cy$_{RL-QN15}$ accelerates cell proliferation during OU repair

OU pathogenesis is closely linked to impaired proliferative activity within the oral epithelium, governed by dynamic interactions between the stratum basale and stratum spinosum (Wu et al., 2010). To assess the pro-regenerative capacity of

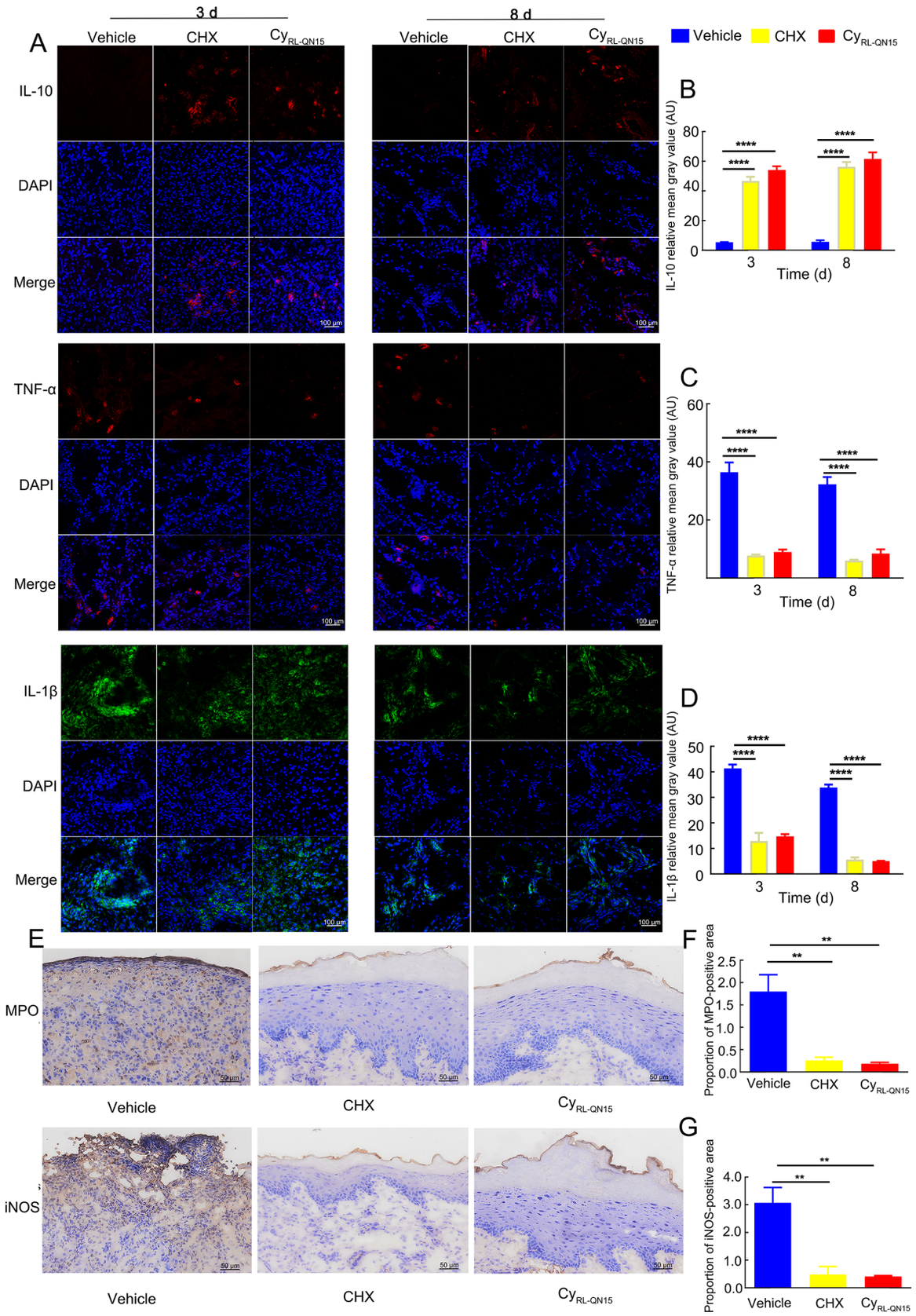

Figure 2 Effects of Cy$_{RL-QN15}$ on cytokine release from macrophages and neutrophils

A: Representative images showing expression and distribution of IL-10 (red), TNF-α (red), and IL-1β (green) in oral mucosa. Scale bar: 100 μm. B–D: Quantitative bar graphs representing mean fluorescence intensity of IL-10, TNF-α, and IL-1β (n=5). Data analyzed by two-way ANOVA with Tukey's multiple comparisons test. E: Representative images showing expression and distribution of MPO and iNOS in oral mucosa at day 8 post-treatment. Scale bar: 50 μm. F, G: Quantitative analysis of MPO-positive and iNOS-positive expression areas (n=5). Data analyzed by one-way ANOVA with Tukey's multiple comparisons test. All data are presented as mean±SEM. **: P<0.01; ****: P<0.0001.

$Cy_{RL\text{-}QN15}$ during the proliferative phase, EdU immunostaining was performed (Figure 3A). On day 3 post-treatment, the $Cy_{RL\text{-}QN15}$ group exhibited a substantial increase in EdU-positive cells localized near the basal layer of the regenerating mucosa (Figure 3B, white dashed line), consistent with successful transition into the proliferative phase. In contrast, the Vehicle group exhibited sparse EdU incorporation and disorganized basal architecture, indicating persistence of the inflammatory phase. By day 8 (Figure 3C), $Cy_{RL\text{-}QN15}$ treatment resulted in robust epithelial proliferation and near-complete re-epithelialization, whereas the Vehicle group displayed incomplete wound closure. These results highlight the capacity of $Cy_{RL\text{-}QN15}$ to accelerate phase transition and enhance mucosal regeneration by stimulating epithelial proliferation.

$Cy_{RL\text{-}QN15}$ regulates cytokine release from oral epithelial cells

Epithelial-derived cytokines are essential regulators of mucosal homeostasis and inflammation (Feliciani et al., 1996). To further explore the regenerative ability of $Cy_{RL\text{-}QN15}$ at the cellular level, primary oral epithelial cells were isolated from SD rat mucosa using sequential enzymatic digestion with dispase II, collagenase I, and hyaluronidase (Figure 4A) (Xie et al., 2021). Cell identity was confirmed by immunostaining for pan-cytokeratin markers (CK14, CK15, CK16, and CK19), which serve as reliable indicators of basal membrane integrity and functional state (Kasai et al., 2016; Xie et al., 2021) (Figure 4B). To establish an *in vitro* inflammatory model, epithelial cells were subjected to LPS challenge (2 μg/mL) for 24 h. RT-qPCR analysis (Figure 4C–E) showed that $Cy_{RL\text{-}QN15}$ significantly attenuated pro-inflammatory responses, with *IL-1β* and *TNF-α* mRNA expression levels reduced to 0.33-fold and 0.61-fold relative to the LPS-only group, respectively. Concurrently, anti-inflammatory *IL-10* expression was up-regulated by 2.58-fold, indicating a shift toward an anti-inflammatory transcriptional profile. These findings implicate $Cy_{RL\text{-}QN15}$ in the attenuation of hyperinflammatory signaling through bidirectional cytokine regulation in oral epithelial cells.

$Cy_{RL\text{-}QN15}$ promotes epithelial proliferation and migration *in vitro*

To systematically evaluate the regenerative activity of $Cy_{RL\text{-}QN15}$, *in vitro* proliferation and migration assays were performed using CCK-8 and Transwell assays. As shown in Figure 5A, B, $Cy_{RL\text{-}QN15}$ enhanced cell migratory capacity in a dose-dependent manner. Compared with the Vehicle group, $Cy_{RL\text{-}QN15}$ treatment at 1, 10, and 100 nmol/L increased the number of migrated cells by 1.73-fold, 2.42-fold, and 3.06-fold, respectively. CCK-8 analysis (Figure 5C) further confirmed that 24 h of exposure to $Cy_{RL\text{-}QN15}$ promoted cell proliferation, with viability enhanced 1.19-fold, 1.31-fold, and 1.42-fold across the same concentration gradient. Together, these results provide mechanistic evidence that $Cy_{RL\text{-}QN15}$ exerts potent and accelerated healing effects by concurrently activating epithelial proliferation and migration.

mRNA sequencing identifies the NF-κB signaling pathway as a key target of $Cy_{RL\text{-}QN15}$

To investigate the molecular mechanism underlying the therapeutic effects of $Cy_{RL\text{-}QN15}$, transcriptomic profiling was conducted on OU tissues harvested from SD rats following 3 days of $Cy_{RL\text{-}QN15}$ treatment. All sequencing data underwent stringent quality control and normalization prior to analysis. Principal component analysis (PCA) revealed distinct transcriptional signatures between the Vehicle and $Cy_{RL\text{-}QN15}$ groups, with tight clustering within each group and notable separation between groups (Figure 6A). Two Vehicle samples showed particularly high intra-group similarity. Differential expression analysis identified 261 DEGs between the $Cy_{RL\text{-}QN15}$ and Vehicle groups, including 207 up-regulated and 54 down-regulated genes (Figure 6B). KEGG pathway enrichment analysis identified 30 significantly enriched pathways, with the top 11 ranked by enrichment score shown in Figure 6C. GO analysis demonstrated DEG enrichment in 18 BP, 12 CC, and seven MF terms. The top 20 most enriched genes within each GO category are presented in Figure 6D. Enriched BP terms included response to peptides and cellular response to LPS; enriched CC terms included keratin filaments and intermediate

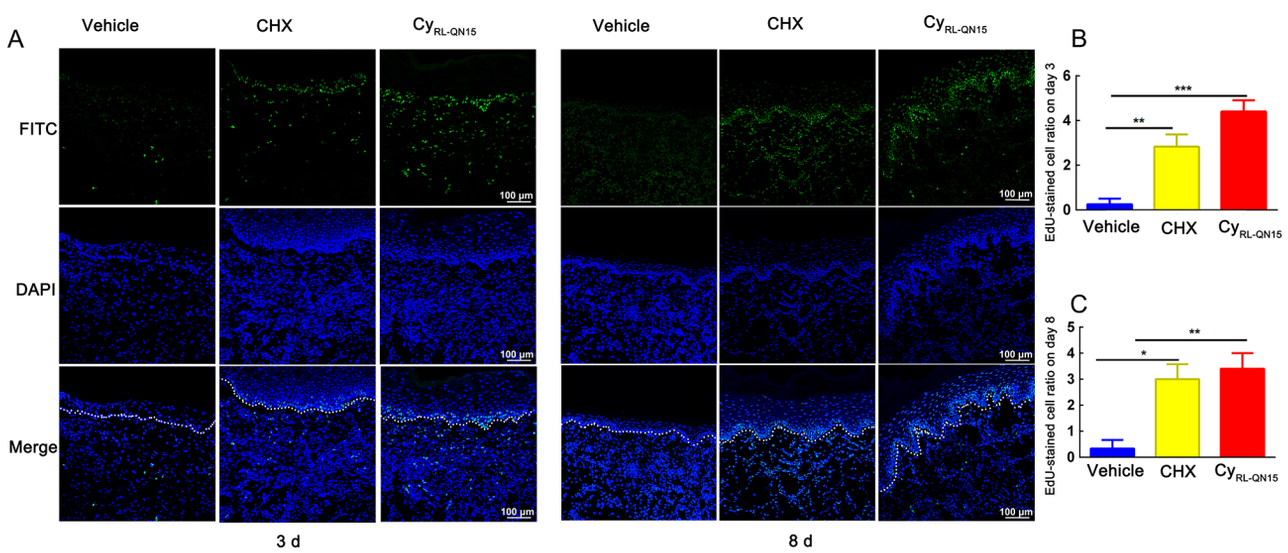

Figure 3 Local application of $Cy_{RL\text{-}QN15}$ promotes cell proliferation in the OU area

A: Representative images of EdU-stained cell (green) on days 3 and 8 post-OU formation. Basal oral mucosal layer is marked by a white dashed line. Scale bar: 100 μm. B: Quantitative bar graph of EdU-stained cell on day 3 post-OU formation. C: Quantitative bar graph of EdU-stained cell on day 8 post-treatment. All data are expressed as mean±SEM, n=5. *: P<0.05; **: P<0.01; ***: P<0.001. Data analyzed by one-way ANOVA with Tukey's multiple comparisons test.

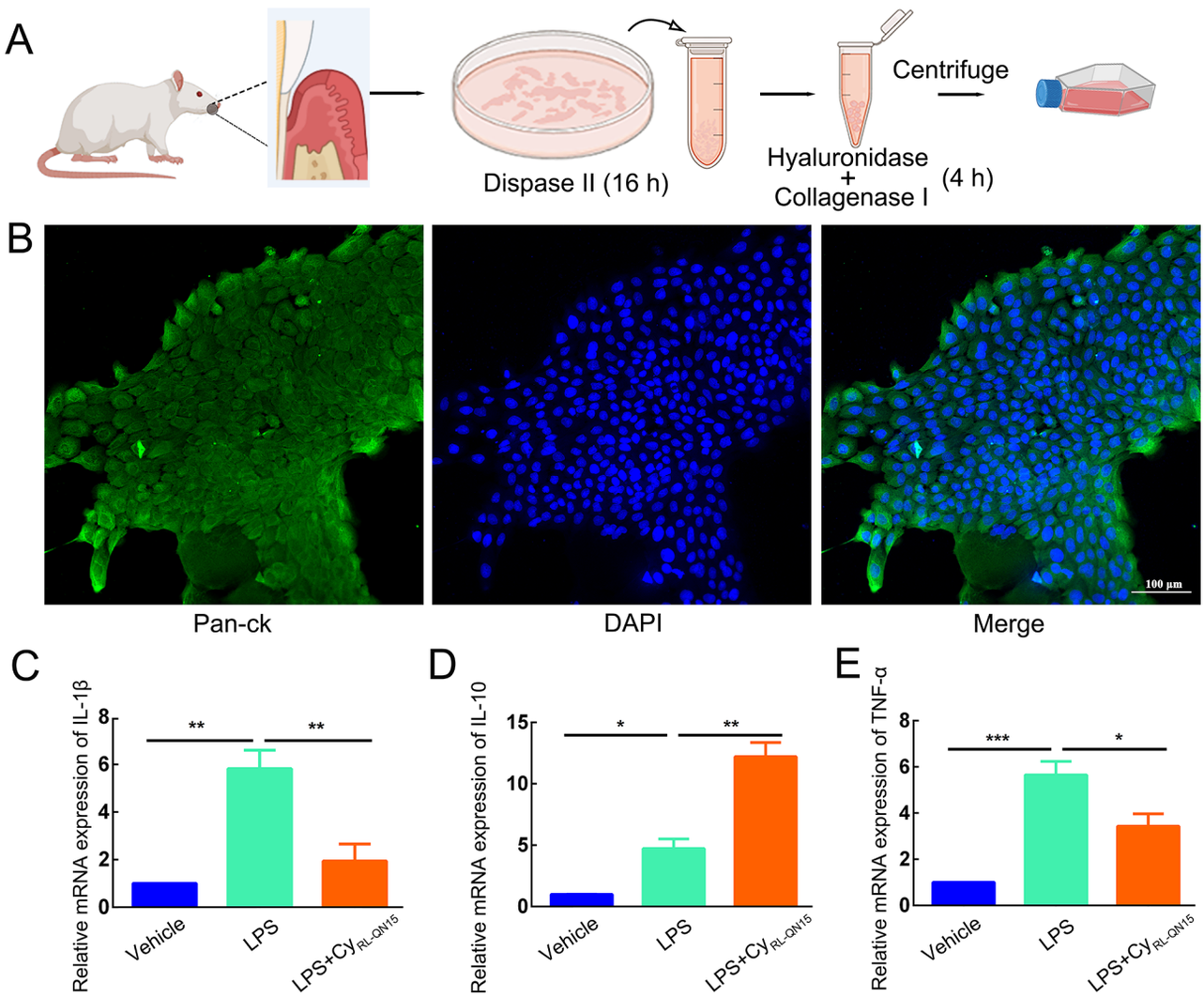

Figure 4 $Cy_{RL\text{-}QN15}$ regulates cytokine release from oral epithelial cells

A: Flowchart of primary oral epithelial cell isolation process. B: Representative immunofluorescence images of pan-CK-labeled positive cells. Scale bar: 100 μm. C–E: Quantitative analysis of mRNA expression levels of *IL-1β*, *TNF-α*, and *IL-10* (n=6). All data are expressed as mean±SEM. *: P<0.05; **: P<0.01; ***: P<0.001. Data analyzed by one-way ANOVA with Tukey's multiple comparisons test.

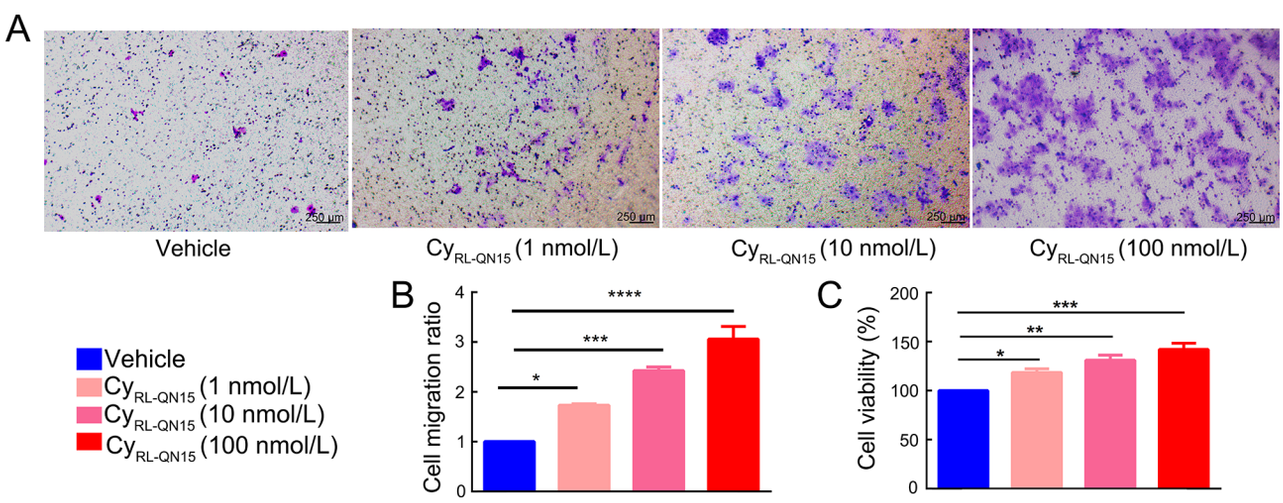

Figure 5 Impact of $Cy_{RL\text{-}QN15}$ on oral epithelial cell proliferation and migration

A: Representative images of oral epithelial cell migration (crystal violet staining). Scale bar: 250 μm. B: Quantitative analysis of $Cy_{RL\text{-}QN15}$ effects on cell migration (n=4). C: Quantitative analysis of $Cy_{RL\text{-}QN15}$ effects on cell proliferation (n=6). Data analyzed by one-way ANOVA with Tukey's multiple comparisons test. All data are expressed as mean±SEM. *: P<0.05; **: P<0.01; ***: P<0.001; ****: P<0.0001.

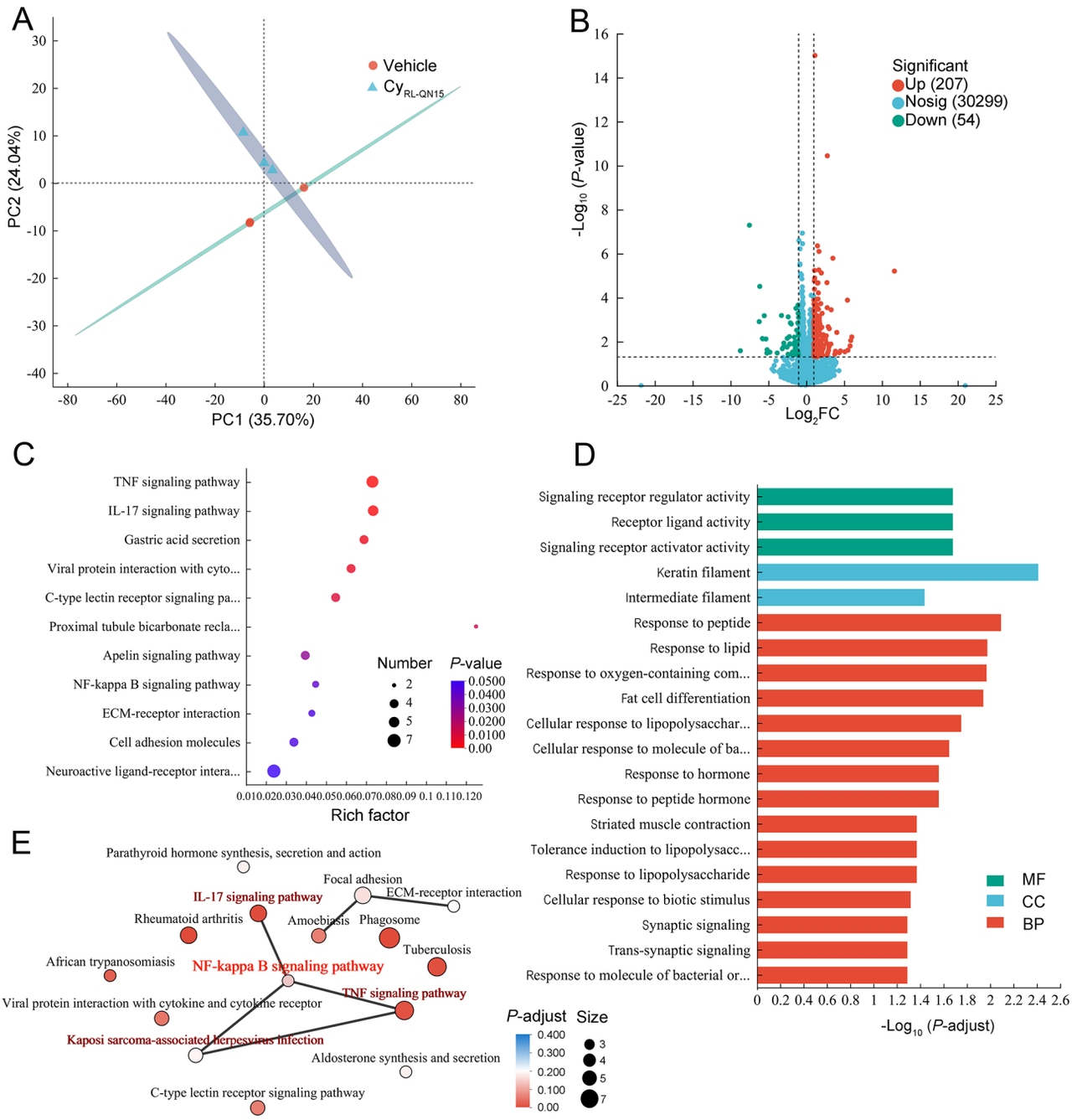

Figure 6 mRNA sequencing of OU mucosa in SD rats

A: Principal component analysis (PCA) demonstrating sample reproducibility. B: Volcano plot showing fold changes (FC) and significance (*P*-value) of differentially expressed genes (DEGs) between $Cy_{RL-QN15}$ and Vehicle groups. Nosig: No significant change. C: Kyoto Encyclopedia of Genes and Genomes (KEGG) pathway enrichment analysis of pathways enriched in DEGs. Size of bubbles represents number of significantly enriched genes within each pathway. Colors indicate level of enrichment significance. D: Gene Ontology (GO) enrichment analysis of biological process (BP), cellular component (CC), and molecular function (MF) terms enriched in DEGs. E: KEGG enrichment network of connections among enriched pathways. Size of circles is proportional to gene count in each pathway. Colors reflect significance of enrichment (adjusted *P*-value) (*n*=3).

filaments; and enriched MF terms included receptor-ligand activity and receptor activator activity. Notably, $Cy_{RL-QN15}$ treatment significantly affected inflammatory signaling, including the TNF and IL-17 pathways. KEGG pathway network analysis revealed that the NF-κB pathway formed the central node of a tightly interconnected regulatory module with the TNF and IL-17 signaling axes (Figure 6E). Disease association analysis using the DisGeNET database (https://disgenet.com) further highlighted TLR4 (Disease Specificity Index, DSI=0.33; Disease Pleiotropy Index, DPI=0.92; associated with 1 476 disease-related genes) and NF-κB (DSI=0.3, DPI=0.92; associated with 1 847 disease-related genes) as critical drivers of OU pathogenesis. These findings align with previous studies implicating the TLR4/MyD88/NF-κB axis in the regulation of oral mucosal inflammation (Ji et al., 2022; Kawai & Akira, 2010; Li et al., 2025a; Zhang et al., 2023a). Given the transcriptomic enrichment of the NF-κB pathway and strong TLR4 association, these results support the hypothesis that $Cy_{RL-QN15}$ exerts its therapeutic effects primarily through suppression of the TLR4/MyD88/NF-κB signaling pathway.

$Cy_{RL\text{-}QN15}$ suppresses MyD88/NF-κB signaling *in vivo* and *in vitro*

Mechanistic studies identified NF-κB as a master molecular switch in inflammation, initiating transcriptional activation of pro-inflammatory mediators through rapid translocation to the nucleus during the early pathogenic phase, establishing the MyD88/NF-κB axis as the central regulatory hub in inflammatory cascades (Guo et al., 2024; Hu et al., 2020; Yu et al., 2020). To delineate the role of this pathway in $Cy_{RL\text{-}QN15}$-mediated OU repair, bidirectional validation was conducted using both an *in vivo* rat model and an *in vitro* LPS-induced oral epithelial cell inflammation model. In the *in vivo* system, western blotting was performed to assess protein expression across Vehicle, CHX, and $Cy_{RL\text{-}QN15}$ treatment groups (Figure 7A–D). Compared with Vehicle, $Cy_{RL\text{-}QN15}$ treatment significantly reduced the expression of MyD88 (0.51-fold), P-IκBα (0.54-fold), and P-P65 (0.65-fold). In the *in vitro* model, $Cy_{RL\text{-}QN15}$ was applied to LPS-challenged oral epithelial cells. RT-qPCR analysis revealed that $Cy_{RL\text{-}QN15}$ significantly down-regulated *MyD88* (0.76-fold), *IκB* (0.45-fold), and *NF-κB* (0.64-fold) mRNA expression relative to the LPS-only group (Figure 7E–G).

$Cy_{RL\text{-}QN15}$ directly interacts with the TLR4 receptor

The pathological progression of OUs is closely associated with TLR4-mediated dysregulation of innate immune activation. Excessive activation of the TLR4/NF-κB signaling axis drives the cascade release of pro-inflammatory cytokines (e.g., TNF-α, IL-1β), forming a critical molecular mechanism for OU development (Elbatreek et al., 2023; Hietanen et al., 2012). To investigate whether $Cy_{RL\text{-}QN15}$ directly targets TLR4, molecular docking and functional validation (MST, CCK-8) analyses were performed. Docking simulations demonstrated strong spatial complementarity between $Cy_{RL\text{-}QN15}$ and the TLR4 binding pocket ($\Delta G_{binding}$=−12.0 kcal/mol) (Figure 8A–C). Key residues at the binding interface included Glu134, Tyr183, Tyr185, and Leu211, with interaction distances below 4 Å (Figure 8D, E). Binding mode analysis revealed electrostatic interactions as the primary driving force, supplemented by hydrogen bonding (yellow dashed lines) with Tyr185 and hydrophobic stabilization by Leu211 (Figure 8F, G).

To analyze the dynamic conformational features of the $Cy_{RL\text{-}QN15}$-TLR4 complex, molecular dynamics simulations were employed. Root mean square deviation (RMSD) trajectories revealed that $Cy_{RL\text{-}QN15}$ maintained a stable conformation at approximately 4 Å throughout the 100 ns simulation (Figure 8H). In contrast, TLR4 exhibited dynamic fluctuations within the range of 1.5–3.5 Å, indicating conformational adaptation of the receptor upon ligand binding. Radius of gyration (Rg) analysis confirmed the structural compactness of both $Cy_{RL\text{-}QN15}$ and TLR4, with no evidence of significant unfolding or compression (Figure 8I). MST quantification revealed a dissociation constant (K_d) of 2.64±0.70 μmol/L for $Cy_{RL\text{-}QN15}$-TLR4 binding (Figure 8J), consistent with the molecular docking-predicted binding free energy (−12 kcal/mol). Functional validation using CCK-8 assays demonstrated that $Cy_{RL\text{-}QN15}$ (100 nmol/L) significantly increased oral epithelial cell viability to 114% compared with the Vehicle group after 24 h. Notably, co-treatment with the TLR4-specific inhibitor TAK-242 (1 μmol/L) substantially attenuated the pro-proliferative effect of $Cy_{RL\text{-}QN15}$, restoring cell viability to baseline levels (102.3%) (Figure 8K). Together, these findings confirm that $Cy_{RL\text{-}QN15}$ exerts its proliferative and anti-inflammatory effects through direct binding to TLR4, thereby suppressing downstream MyD88/NF-κB signaling.

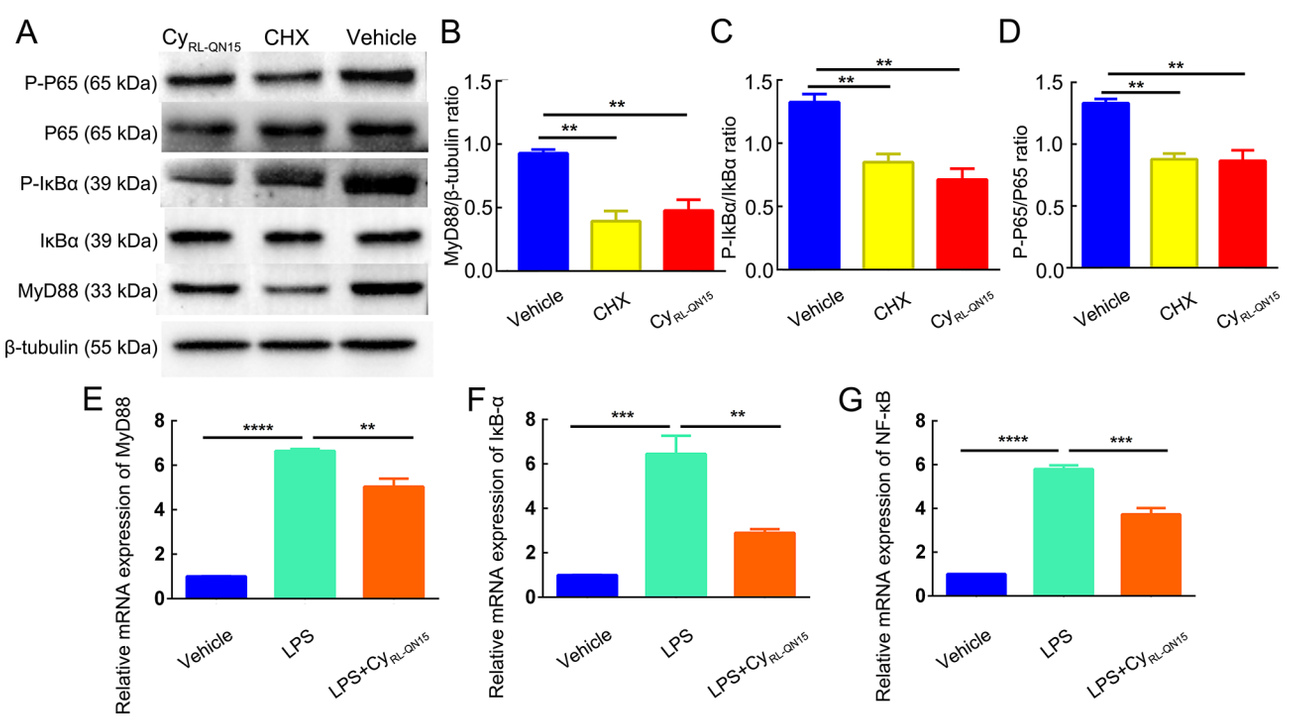

Figure 7 $Cy_{RL\text{-}QN15}$ inhibits MyD88/NF-κB signaling *in vivo* and *in vitro*

A: Representative western blot images of MyD88/NF-κB signaling pathway components (MyD88, IκB, P65). B–D: Quantitative analysis of MyD88, P-IκB, and P-P65 protein expression. β-Tubulin served as an internal reference (n=5). E–G: Quantitative analysis of *MyD88*, *IκB*, and *P65* mRNA expression. *GAPDH* was used as an internal reference (n=6). All data are expressed as mean±SEM. **: P<0.01; ***: P<0.001; ****: P<0.0001. Data analyzed by one-way ANOVA with Tukey's multiple comparisons test.

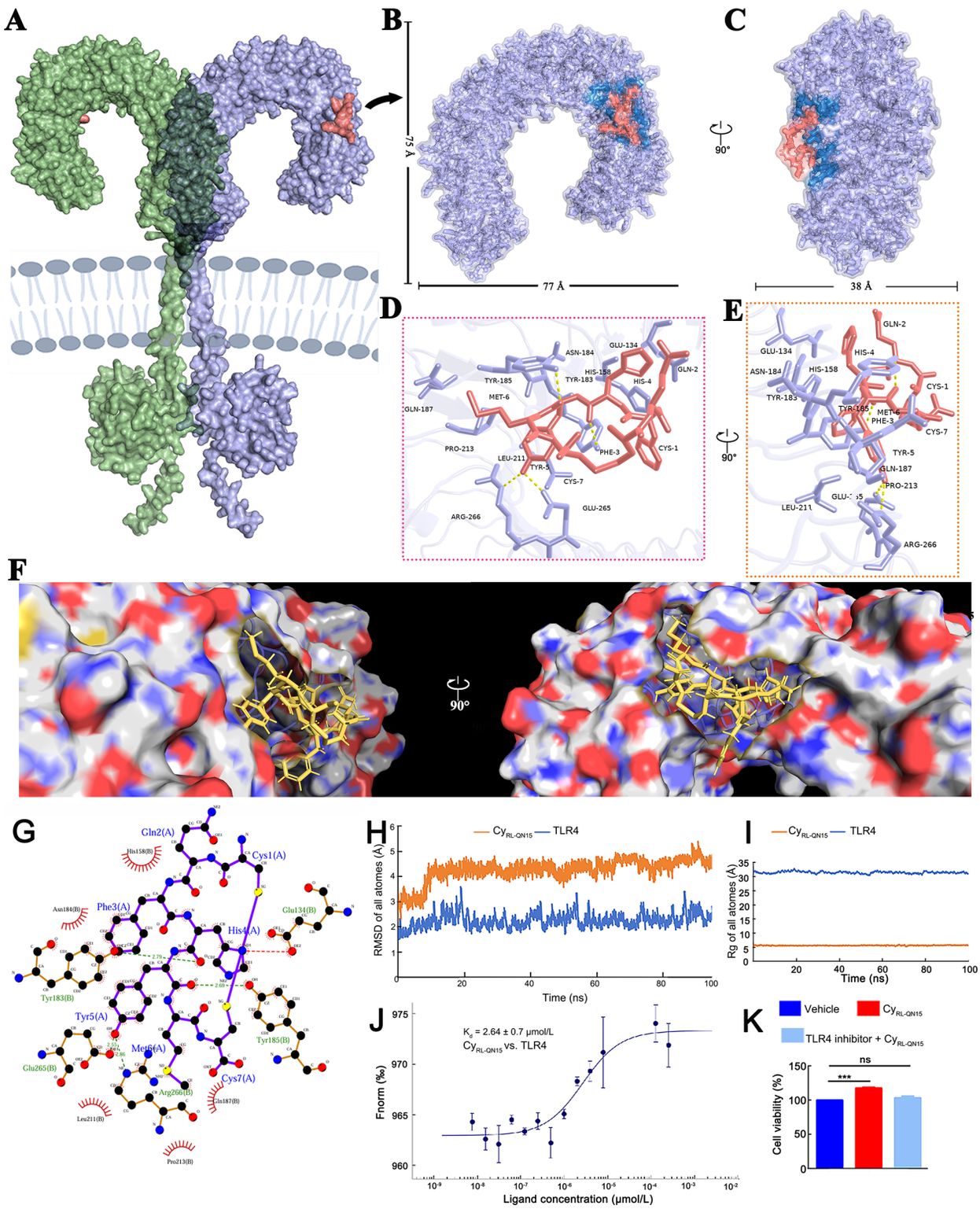

Figure 8 $Cy_{RL\text{-}QN15}$ directly binds to the TLR4 receptor

A: Overall 3D structure of the $Cy_{RL\text{-}QN15}$-TLR4 complex. TLR4 homodimer shown in surface representation (green and purple) with $Cy_{RL\text{-}QN15}$ (orange ribbon) bound to the extracellular domain (ECD) of TLR4. Intracellular domain (ICD) of TLR4 is located in the cytoplasmic region. B, C: Complementary binding pockets between the TLR4 ECD (purple) and $Cy_{RL\text{-}QN15}$ (orange) with interaction surface in blue: front view (B), side view (C). D, E: Views of $Cy_{RL\text{-}QN15}$-TLR4 binding interface: Hydrogen bonds are indicated by yellow dashed lines, front view (D), side view (E). F: Extended views of $Cy_{RL\text{-}QN15}$-TLR4 binding sites. $Cy_{RL\text{-}QN15}$ is represented by the stick model (yellow). G: 2D schematic of key TLR4 residues interacting with $Cy_{RL\text{-}QN15}$, showing hydrogen bonds (green dashed lines) and corresponding bond lengths (Å). H: Molecular dynamics trajectory analysis showing time-dependent evolution of root mean square deviation (RMSD) for $Cy_{RL\text{-}QN15}$ (orange) and TLR4 (blue). I: Dynamic profile of radius of gyration (Rg) profiles over time. J: Binding affinity measurement by MST, showing the equilibrium dissociation constant between $Cy_{RL\text{-}QN15}$ and TLR4 (K_d). K: CCK-8 assay validation of TLR4-$Cy_{RL\text{-}QN15}$ interaction (n=6). All data are expressed as mean±SEM. ***: P<0.001; ns: Not significant. Data analyzed by one-way ANOVA with Tukey's multiple comparisons test.

Key amino acid residues mediate $Cy_{RL\text{-}QN15}$ binding to the TLR4 receptor

To define the structural basis of $Cy_{RL\text{-}QN15}$ binding to TLR4 and guide ligand optimization strategies, residue energy decomposition analysis was conducted. Among the residues comprising $Cy_{RL\text{-}QN15}$, His4, Tyr5, and Met6 contributed most significantly to binding free energy (ΔG=−2.7, −4.3, and −2.0 kcal/mol, respectively), suggesting critical roles in ligand-receptor recognition via hydrogen bonding (His4, Tyr5) or hydrophobic interactions (Met6).

As shown in Figure 9A, B, alanine-scanning mutagenesis was used to validate these predictions by individually substituting these residues with alanine (Ala)—an inert residue with methyl side chains capable of attenuating site-specific interactions, commonly employed to assess the functional contribution of individual residues (Li et al., 2024c). Molecular docking of the mutant peptides revealed significant reprogramming of binding modes: the binding site shifted to the receptor transmembrane domain, with complete loss of N-terminal binding capacity compared to wild-type $Cy_{RL\text{-}QN15}$. Three mutants—CYM1 (His4A), CYM2 (Tyr5A), and CYM3 (Met6A)—were subsequently generated via site-directed Ala mutagenesis (Supplementary Table S3). Western blot analysis demonstrated that compared with wild-type $Cy_{RL\text{-}QN15}$, treatment with CYM1 and CYM3 significantly reduced the inhibitory effect on the TLR4/NF-κB signaling pathway (Figure 9C–F). Quantitative analysis further revealed that MyD88 expression in the CYM1 and CYM3 groups increased by 1.32-fold and 1.28-fold, respectively, while P-IκBα levels increased by 3.05-fold and 2.47-fold and P-P65 expression increased by 3.12-fold and 2.03-fold. Collectively, these findings identify His4 and Met6 as core functional residues responsible for $Cy_{RL\text{-}QN15}$-mediated immunosuppression.

MST assays further quantified the binding affinity of mutants to TLR4 (Figure 9G–I). As shown in Table S3, CYM3 exhibited a K_d of 90.58±1.31 μmol/L (35-fold higher than wild-type $Cy_{RL\text{-}QN15}$), while CYM1 showed a K_d of 24.69±2.92 μmol/L (10-fold increase over wild-type). These data confirm that Met6 mutation severely impairs peptide-receptor binding, highlighting its essential role in target engagement. Collectively, these findings demonstrate that $Cy_{RL\text{-}QN15}$ inhibits MyD88/NF-κB signaling primarily through Met6-mediated binding to TLR4, providing mechanistic insight for future structure–function optimization.

DISCUSSION

OUs are prevalent oral mucosal lesions affecting approximately 2.5 billion individuals worldwide (Cheng et al., 2023), frequently manifesting as pain erosions accompanied by dysesthesia and, in 25% of cases, dysgeusia (Elbatreek et al., 2023). Severe forms compromise both physiological and psychological health. Effective resolution of OU requires orchestrated progression through hemostasis, inflammation, proliferation, and remodeling phases, with timely transition from inflammation to proliferation serving as a critical therapeutic target (Mays et al., 2012). Despite advances in symptomatic management, current treatment modalities offer limited efficacy. For instance, anthocyanins exert dual anti-inflammatory and pro-proliferative effects but require co-administration with 5-fluorouracil for therapeutic benefit (Tancharoen et al., 2018); leptin facilitates epithelial cell migration without improving proliferative capacity (Umeki et al., 2014); and morphine exerts pro-proliferative and pro-migratory effects at low doses but antagonistic activity at higher doses (>10 μmol/L) (Charbaji et al., 2012). Consequently, the development of efficient and safe mucosal

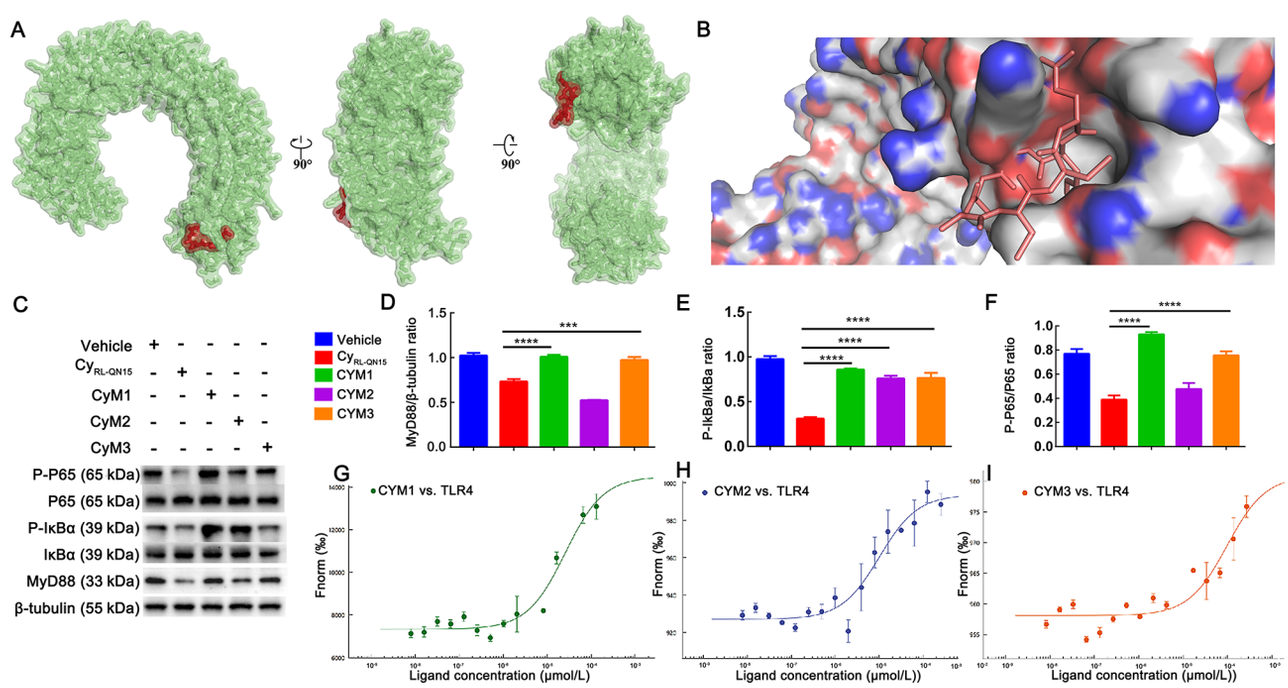

Figure 9 Key amino acid residues involved in the binding of $Cy_{RL\text{-}QN15}$ to the TLR4 receptor

A: Front, side, and top views of overall topology of the $Cy_{RL\text{-}QN15}$ mutant-TLR4 complex. Mutant (red model) binds near the transmembrane domain of the TLR4 monomer (green model). B: Extended view of the binding site in the mutant-TLR4 complex, with the stick model (red) representing the $Cy_{RL\text{-}QN15}$ mutant. C: Western blot analysis of mutant effects on NF-κB signaling pathway activation. D–F: Quantitative analysis of protein expression levels for MyD88, P-IκBα, and P-P65 (n=5). G–I: Linear regression plots of binding affinity between $Cy_{RL\text{-}QN15}$ and TLR4 protein. All data are expressed as mean±SEM. ***: P<0.001; ****: P<0.0001. Data analyzed by one-way ANOVA with Tukey's multiple comparisons test.

repair agents remains an urgent clinical priority.

$Cy_{RL\text{-}QN15}$, a seven-residue, ultra-short cyclic derivative of RL-QN15, has emerged as a promising candidate in this context. Previous studies have demonstrated its reparative efficacy across diverse tissue types, including skin wound healing, diabetic foot ulcer regeneration, and hair follicle neogenesis (Fu et al., 2022; Jia et al., 2024; Li et al., 2025b; Wu et al., 2024). Unlike bioactive peptides such as cathelicidin-OA1 and Andersonin-W1, which also demonstrate wound-healing capabilities, $Cy_{RL\text{-}QN15}$ exhibits enhanced biostability due to its compact cyclic architecture, providing a structural basis for maintaining functional activity in complex physiological environments (Cao et al., 2018; Li et al., 2024a).

Building on these findings, $Cy_{RL\text{-}QN15}$ was evaluated in the current study for its therapeutic efficacy in oral mucosal repair, addressing the current lack of data on ultra-short cyclic peptides in this context. In a rat model oral ulceration, $Cy_{RL\text{-}QN15}$ (100 nmol/L) significantly enhanced tissue regeneration compared to the conventional positive control CHX (2 mmol/L). $Cy_{RL\text{-}QN15}$ suppressed inflammation by regulating cytokine release from macrophages and neutrophils, thereby establishing a microenvironment conducive to healing. Simultaneously, it promoted epithelial proliferation and migration toward the wound edge, accelerating re-epithelialization and tissue remodeling. Histological analysis revealed pronounced epithelial thickening following $Cy_{RL\text{-}QN15}$ treatment, consistent with active mucosal regeneration (Wakamori et al., 2022). Transcriptomic profiling identified significant enrichment of NF-κB-related genes, analogous to the mechanisms reported for established mucosal therapeutics such as Danshen, Qingwei San, dioscin, and naltrexone (Diaz et al., 2024; Jin et al., 2022; Li et al., 2020; Shi et al., 2022). Mechanistically, $Cy_{RL\text{-}QN15}$ acted by directly binding to TLR4, a key receptor in innate immunity, to suppress downstream MyD88/NF-κB signaling and accelerate the transition from inflammation to proliferation. Molecular docking and dynamic simulations indicated that $Cy_{RL\text{-}QN15}$ formed stable hydrogen bonds and hydrophobic interactions with critical residues (Glu-134, Tyr-183, Tyr-185, Leu-211) in the extracellular domain of TLR4, inducing adaptive conformational changes in the receptor. MST confirmed this direct interaction, and pharmacological blockade of TLR4 impaired $Cy_{RL\text{-}QN15}$-mediated repair, validating TLR4 as the key target. Site-directed mutagenesis experiments further identified Met6 as a critical functional residue, with the Met6-substituted variant CYM3 exhibiting a 35-fold reduction in TLR4 binding affinity relative to the wild-type peptide.

Compared with traditional TLR4 antagonists such as purpurolide C, ginsenoside Rh2, and eritoran tetrasodium, which primarily target the TLR4-myeloid differentiation factor 2 (MD2) complex and are constrained by high structural specificity, synthetic complexity, and substantial off-target risks (Liu et al., 2023; Pan et al., 2024; Shirey et al., 2013), $Cy_{RL\text{-}QN15}$ binds directly to the extracellular domain of TLR4, bypassing MD2 and avoiding limitations associated with MD2-dependent antagonism. This mechanism aligns with the strategy of newer TLR4-targeted agents such as TAK-242 (Liu et al., 2024a; Takashima et al., 2009). Although originally thought to act through selective binding to the murine TLR4 transmembrane Cys747 site to induce receptor inactivation, subsequent evidence from a murine psoriasis model indicated that TAK-242 interacts with extracellular residues Glu509, Gln510, and Ser534 instead. This discrepancy highlights the structural and functional complexity of TLR4 inhibition and the need for further mechanistic validation (Liu et al., 2024; Takashima et al., 2009). Additionally, compared to other peptide-based TLR4 antagonists such as NA39—a 39 amino acid peptide that disrupts MD2-TLR4 dimerization through an incompletely characterized mechanism (Li et al., 2024d)—and SPS4, which inhibits TLR4-MD2 dimerization but fails to promote anti-inflammatory cytokine secretion or enhance cell viability (Awasthi et al., 2021), $Cy_{RL\text{-}QN15}$ not only efficiently antagonizes TLR4-mediated inflammation but also achieves dual reparative functions through its pro-proliferative and pro-migratory effects on epithelial cells.

Identification of Met6 as a critical residue for the anti-inflammatory and pro-healing activity of $Cy_{RL\text{-}QN15}$ aligns with prior research on Met-containing peptides. For example, the Met-Met dipeptide has been shown to exert anti-inflammatory effects by inhibiting the MAPK/NF-κB pathway (Chen et al., 2022; Lan et al., 2020), while L-methionine (L-Met) has been shown to directly suppress NF-κB signaling (Wang et al., 2022) and D-methionine (D-Met) alleviates radiation-induced oral mucositis by modulating oxidative stress (Wu et al., 2019). These connections provide new insights into deciphering the shared molecular targets and signaling pathways underlying the anti-inflammatory functions of Met-containing peptides.

This study also lays a scientific foundation for investigating combinatorial strategies involving natural polysaccharides such as hyaluronic acid and chitosan. Hyaluronic acid retains water to maintain a hydrated wound microenvironment and may prolong local peptide availability when co-administered with $Cy_{RL\text{-}QN15}$. Chitosan, a cationic and biocompatible carrier, enables stable peptide complexation and may enhance bioavailability and targeted accumulation of $Cy_{RL\text{-}QN15}$ at the wound site (Chhillar & Jaiswal, 2025; Zhang et al., 2024).

Notwithstanding the promising nature of these findings, several limitations warrant consideration. First, while $Cy_{RL\text{-}QN15}$ promoted oral epithelial cell proliferation and migration, further research is required to assess whether it exerts similar effects on tumor growth. Second, the sample size was relatively small, underscoring the need for large-scale validation, particularly through Phase III clinical trials, to confirm the efficacy and safety of $Cy_{RL\text{-}QN15}$. Third, the precise relationship between $Cy_{RL\text{-}QN15}$ and MD2 remains unclear, and further studies are required to clarify potential interactions.

CONCLUSIONS

This study established $Cy_{RL\text{-}QN15}$ as the first ultra-short cyclic peptide to function as a TLR4 antagonist, exhibiting potent therapeutic effects in OU healing. Through coordinated suppression of inflammation and stimulation of mucosal regeneration, $Cy_{RL\text{-}QN15}$ represents a promising candidate for oral tissue repair. These findings provide a framework for advancing peptide-based therapeutics, supporting future efforts in structural refinement, scalable production, and translational development of small-molecule bioactive peptides for clinical management of mucosal injuries.

SUPPLEMENTARY DATA

Supplementary data to this article can be found online.

COMPETING INTERESTS

The authors declare that they have no competing interests.

AUTHORS' CONTRIBUTIONS

X.W.Y. conceived the project. X.W.Y. and Y.W. provided detailed feedback on the project. N.X.L. supervised the research with assistance from L.H. Z.Q.R. and Y.T.W. designed the experiments. Y.L.Y. and Y.P. contributed to the OU model in SD rats. J.Y.W. and Z.F. were responsible for the extraction of primary oral epithelial cells with support from W.R.S. Q.Y.J. contributed to the *in vivo* studies with support from Y.S.L. M.F.Y. and C.X.L. conducted the *in vitro* studies with assistance from J.T. and Y.F. C.Y.Y. and Y.T.Y. contributed to quantitative analysis with support from Y.J.L. and M.L. Z.Q.R. and X.W.Y. wrote and revised the manuscript. All authors read and approved the final version of the manuscript.

ACKNOWLEDGMENTS

The authors thank the members of their research team for helpful comments and technical assistance.

REFERENCES

Addy M. 1977. Hibitane in the treatment of aphthous ulceration. *Journal of Clinical Periodontology*, **4**(5): 108–116.

Al-Omiri MK, Karasneh J, Alhijawi MM, et al. 2015. Recurrent aphthous stomatitis (RAS): a preliminary within-subject study of quality of life, oral health impacts and personality profiles. *Journal of Oral Pathology & Medicine*, **44**(4): 278–283.

An HW, Mamuti M, Wang XF, et al. 2021. Rationally designed modular drug delivery platform based on intracellular peptide self-assembly. *Exploration* (*Beijing, China*), **1**(2): 20210153.

Awasthi S, Kumar G, Ramani V, et al. 2021. Mechanism of anti-inflammatory activity of TLR4-interacting SPA4 peptide. *ImmunoHorizons*, **5**(8): 659–674.

Ayoub N, Badr N, Al-Ghamdi SS, et al. 2022. HPLC/MS^n profiling and healing activity of a muco-adhesive formula of *Salvadora persica* against acetic acid-induced oral ulcer in rats. *Nutrients*, **14**(1): 28.

Cao XQ, Wang Y, Wu CY, et al. 2018. Cathelicidin-OA1, a novel antioxidant peptide identified from an amphibian, accelerates skin wound healing. *Scientific Reports*, **8**(1): 943.

Cha LN, Yang J, Gao JA, et al. 2024. Bat-derived oligopeptide LE6 inhibits the contact-kinin pathway and harbors anti-thromboinflammation and stroke potential. *Zoological Research*, **45**(5): 1001–1012.

Charbaji N, Schäfer-Korting M, Küchler S. 2012. Morphine stimulates cell migration of oral epithelial cells by delta-opioid receptor activation. *PLoS One*, **7**(8): e42616.

Chen XH, Sun LL, Li DL, et al. 2022. Green tea peptides ameliorate diabetic nephropathy by inhibiting the TGF-β/Smad signaling pathway in mice. *Food & Function*, **13**(6): 3258–3270.

Cheng YO, Veettil SK, Syeed MS, et al. 2023. Comparative efficacy of therapeutic interventions for the management of recurrent aphthous ulcers: a systematic review and network meta-analysis. *Journal of Evidence-Based Dental Practice*, **23**(4): 101918.

Chhillar A, Jaiswal A. 2025. Hyaluronic acid-based self-healing hydrogels for diabetic wound healing. *Advanced Healthcare Materials*, **14**(4): 2404255.

da Silveira Teixeira D, de Figueiredo MAZ, Cherubini K, et al. 2019. The topical effect of chlorhexidine and povidone-iodine in the repair of oral wounds. A review. *Stomatologija*, **21**(2): 35–41.

Darveau RP, Curtis MA. 2021. Oral biofilms revisited: a novel host tissue of bacteriological origin. *Periodontology*, **86**(1): 8–13.

Diaz LC, de Barros Silva PG, Dantas TS, et al. 2024. Naltrexone accelerated oral traumatic ulcer healing and downregulated TLR-4/NF-κB pathway in Wistar rats. *Archives of Oral Biology*, **166**: 106047.

Dudding T, Haworth S, Lind PA, et al. 2019. Genome wide analysis for mouth ulcers identifies associations at immune regulatory loci. *Nature Communications*, **10**(1): 1052.

Elbatreek MH, Fathi AM, Mahdi I, et al. 2023. *Thymus satureioides* Coss. combats oral ulcer via inhibition of inflammation, proteolysis, and apoptosis. *Inflammopharmacology*, **31**(5): 2557–2570.

El-Zahar H, Menze ET, Handoussa H, et al. 2022. UPLC-PDA-MS/MS profiling and healing activity of polyphenol-rich fraction of *Alhagi maurorum* against oral ulcer in rats. *Plants* (*Basel, Switzerland*), **11**(3): 455.

Feliciani C, Gupta AK, Sauder DN. 1996. Keratinocytes and cytokine/growth factors. *Critical Reviews in Oral Biology & Medicine*, **7**(4): 300–318.

Fu Z, Sun HL, Wu YT, et al. 2022. A cyclic heptapeptide-based hydrogel boosts the healing of chronic skin wounds in diabetic mice and patients. *NPG Asia Materials*, **14**(1): 99.

Fujisawa K, Miyamoto Y, Nagayama M. 2003. Basic fibroblast growth factor and epidermal growth factor reverse impaired ulcer healing of the rabbit oral mucosa. *Journal of Oral Pathology & Medicine*, **32**(6): 358–366.

Gang D, Kim DW, Park HS. 2018. Cyclic peptides: promising scaffolds for biopharmaceuticals. *Genes*, **9**(11): 557.

Groeger S, Meyle J. 2019. Oral mucosal epithelial cells. *Frontiers in Immunology*, **10**: 208.

Guo Q, Jin YZ, Chen XY, et al. 2024. NF-κB in biology and targeted therapy: new insights and translational implications. *Signal Transduction and Targeted Therapy*, **9**(1): 53.

Hietanen J, Häyrinen-Immonen R, Al-Samadi A, et al. 2012. Recurrent aphthous ulcers—a Toll-like receptor-mediated disease?. *Journal of Oral Pathology & Medicine*, **41**(2): 158–164.

Hitomi S, Ono K, Yamaguchi K, et al. 2016. The traditional Japanese medicine hangeshashinto alleviates oral ulcer-induced pain in a rat model. *Archives of Oral Biology*, **66**: 30–37.

Hu NH, Wang C, Dai XY, et al. 2020. Phillygenin inhibits LPS-induced activation and inflammation of LX2 cells by TLR4/MyD88/NF-κB signaling pathway. *Journal of Ethnopharmacology*, **248**: 112361.

Hu ZW, Chen YM, Gao M, et al. 2023. Novel strategy for primary epithelial cell isolation: combination of hyaluronidase and collagenase I. *Cell Proliferation*, **56**(1): e13320.

Ji L, Hao SY, Wang JT, et al. 2022. Roles of Toll-like receptors in radiotherapy- and chemotherapy-induced oral mucositis: a concise review. *Frontiers in Cellular and Infection Microbiology*, **12**: 831387.

Ji XJ, Nielsen AL, Heinis C. 2024. Cyclic peptides for drug development. *Angewandte Chemie International Edition*, **63**(3): e202308251.

Jia QY, Fu Z, Li YS, et al. 2024. Hydrogel loaded with peptide-containing nanocomplexes: symphonic cooperation of photothermal antimicrobial nanoparticles and prohealing peptides for the treatment of infected wounds. *ACS Applied Materials & Interfaces*, **16**(11): 13422–13438.

Jin SZ, Guan TX, Wang S, et al. 2022. Dioscin alleviates cisplatin-induced mucositis in rats by modulating gut microbiota, enhancing intestinal barrier function and attenuating TLR4/NF-κB signaling cascade. *International Journal of Molecular Sciences*, **23**(8): 4431.

Joorabloo A, Liu TQ. 2024. Recent advances in reactive oxygen species scavenging nanomaterials for wound healing. *Exploration* (*Beijing, China*), **4**(3): 20230066.

Kasai Y, Sugiyama H, Takagi R, et al. 2016. Brush biopsy of human oral mucosal epithelial cells as a quality control of the cell source for fabrication of transplantable epithelial cell sheets for regenerative medicine. *Regenerative Therapy*, **4**: 71–77.

Kawai T, Akira S. 2010. The role of pattern-recognition receptors in innate immunity: update on Toll-like receptors. *Nature Immunology*, **11**(5): 373–384.

Lan W, Wang Z, Liu JX, et al. 2020. Methionyl-methionine exerts anti-inflammatory effects through the JAK2-STAT5-NF-κB and MAPK signaling pathways in bovine mammary epithelial cells. *Journal of Agricultural and Food Chemistry*, **68**(47): 13742–13750.

Landén NX, Li DQ, Ståhle M. 2016. Transition from inflammation to proliferation: a critical step during wound healing. *Cellular and Molecular Life Sciences*, **73**(20): 3861–3885.

Levin A, Hakala TA, Schnaider L, et al. 2020. Biomimetic peptide self-assembly for functional materials. *Nature Reviews Chemistry*, **4**(11): 615–634.

Li C, Xiong YX, Fu Z, et al. 2024a. The direct binding of bioactive peptide Andersonin-W1 to TLR4 expedites the healing of diabetic skin wounds. *Cellular & Molecular Biology Letters*, **29**(1): 24.

Li DQ, Liu Z, Zhang LT, et al. 2024b. The lncRNA *SNHG26* drives the inflammatory-to-proliferative state transition of keratinocyte progenitor cells during wound healing. *Nature Communications*, **15**(1): 8637.

Li JW, Wang LM, Zhang N, et al. 2024c. Enzyme and pathway engineering for improved betanin production in *Saccharomyces cerevisiae*. *ACS Synthetic Biology*, **13**(6): 1916–1924.

Li RH, Tang YZ, Chen ZN, et al. 2024d. Screening TLR4 binding peptide from *Naja atra* venom glands based on phage display. *Toxins*, **16**(3): 113.

Li SY, Yang P, Ding XF, et al. 2022a. Puerarin improves diabetic wound healing via regulation of macrophage M2 polarization phenotype. *Burns & Trauma*, **10**: tkac046.

Li WJ, Chen Y, Li KL, et al. 2025a. *Periplaneta americana* extract improves recurrent oral ulcers through regulation of TLR4/NF-κB and Nrf2/HO-1 pathways. *Scientific Reports*, **15**(1): 8578.

Li WJ, Wang KX, Liu YD, et al. 2022b. A novel drug combination of mangiferin and cinnamic acid alleviates rheumatoid arthritis by inhibiting TLR4/NFκB/NLRP3 activation-induced pyroptosis. *Frontiers in Immunology*, **13**: 912933.

Li XX, Zheng XT, Liu ZJ, et al. 2020. Cryptotanshinone from *Salvia miltiorrhiza* bunge (Danshen) inhibited inflammatory responses via TLR4/MyD88 signaling pathway. *Chinese Medicine*, **15**: 20.

Li YS, Jia QY, Liu NX, et al. 2025b. Peptide RL-QN15 regulates functions of epidermal stem cells to accelerate skin wound regeneration via the FZD8/β-catenin axis. *Exploration*, 20240090.

Li ZY, Wang C, Wang ZY, et al. 2019. Allele-selective lowering of mutant HTT protein by HTT-LC3 linker compounds. *Nature*, **575**(7781): 203–209.

Liu LJ, Zhang HL, Tang XR, et al. 2024a. Geniposide ameliorates psoriatic skin inflammation by inhibiting the TLR4/MyD88/NF-κB p65 signaling pathway and MMP9. *International Immunopharmacology*, **133**: 112082.

Liu MD, Huo XY, Li CC, et al. 2024b. Oxypeucedanin hydrate alleviates rheumatoid arthritis by inhibiting the TLR4-MD2/NF-κB/MAPK signaling axis. *Acta Biochimica et Biophysica Sinica*, **56**(12): 1789–1801.

Liu NX, Meng BL, Zeng L, et al. 2020. Discovery of a novel rice-derived peptide with significant anti-gout potency. *Food & Function*, **11**(12): 10542–10553.

Liu YT, Xia GY, Chen YY, et al. 2023. Purpurolide C-based microneedle promotes macrophage-mediated diabetic wound healing *via* inhibiting TLR4-MD2 dimerization and MyD88 phosphorylation. *Acta Pharmaceutica Sinica B*, **13**(12): 5060–5073.

Lukova OA, Zaslavskaya MI, Makhrova TV, et al. 2020. Expression of toll-like and adhesive receptors on epithelial cells of the oral mucosa in periodontitis. *Klinicheskaia Laboratornaia Diagnostika*, **65**(10): 645–648.

Mays JW, Sarmadi M, Moutsopoulos NM. 2012. Oral manifestations of systemic autoimmune and inflammatory diseases: diagnosis and clinical management. *Journal of Evidence Based Dental Practice*, **12**(3 Suppl): 265–282.

Ni M. 2019. Ultrashort peptides: minimum number in amino acid residues, maximum number in bioapplications. *Revista Bionatura*, **4**(1): 1.

Pan SJ, Peng LY, Yi Q, et al. 2024. Ginsenoside Rh_2 alleviates LPS-induced inflammatory responses by binding to TLR_4/MD-2 and blocking TLR_4 dimerization. *International Journal of Molecular Sciences*, **25**(17): 9546.

Rakhorst HA, Tra WMW, Posthumus-van Sluijs SJ, et al. 2006. Mucosal keratinocyte isolation: a short comparative study on thermolysin and dispase. *International Journal of Oral and Maxillofacial Surgery*, **35**(10): 935–940.

Şenel S. 2021. An overview of physical, microbiological and immune barriers of oral mucosa. *International Journal of Molecular Sciences*, **22**(15): 7821.

Seow WY, Hauser CAE. 2014. Short to ultrashort peptide hydrogels for biomedical uses. *Materials Today*, **17**(8): 381–388.

Sharifiaghdam M, Shaabani E, Faridi-Majidi R, et al. 2022. Macrophages as a therapeutic target to promote diabetic wound healing. *Molecular Therapy*, **30**(9): 2891–2908.

Shi J, Wang LY, Zhang YS, et al. 2021. Clinical efficacy of vitamin B in the treatment of mouth ulcer: a systematic review and meta-analysis. *Annals of Palliative Medicine*, **10**(6): 6588–6596.

Shi L, An YC, Cheng L, et al. 2022. Qingwei San treats oral ulcer subjected to stomach heat syndrome in db/db mice by targeting TLR4/MyD88/NF-κB pathway. *Chinese Medicine*, **17**(1): 1.

Shirey KA, Lai W, Scott AJ, et al. 2013. The TLR4 antagonist Eritoran protects mice from lethal influenza infection. *Nature*, **497**(7450): 498–502.

Ślebioda Z, Szponar E, Kowalska A. 2014. Etiopathogenesis of recurrent aphthous stomatitis and the role of immunologic aspects: literature review. *Archivum Immunologiae et Therapiae Experimentalis*, **62**(3): 205–215.

Summers SA, Hoi A, Steinmetz OM, et al. 2010. TLR9 and TLR4 are required for the development of autoimmunity and lupus nephritis in pristane nephropathy. *Journal of Autoimmunity*, **35**(4): 291–298.

Sun DD, Guo K, Liu NX, et al. 2023. Peptide RL-QN15 promotes wound healing of diabetic foot ulcers through p38 mitogen-activated protein kinase and smad3/miR-4482–3p/vascular endothelial growth factor B axis. *Burns & Trauma*, **11**: tkad035.

Sun HL, Wang Y, He TT, et al. 2021. Hollow polydopamine nanoparticles loading with peptide RL-QN15: a new pro-regenerative therapeutic agent for skin wounds. *Journal of Nanobiotechnology*, **19**(1): 304.

Takashima K, Matsunaga N, Yoshimatsu M, et al. 2009. Analysis of binding site for the novel small-molecule TLR4 signal transduction inhibitor TAK-242 and its therapeutic effect on mouse sepsis model. *British Journal of Pharmacology*, **157**(7): 1250–1262.

Tancharoen S, Shakya P, Narkpinit S, et al. 2018. Anthocyanins extracted from *Oryza sativa* L. prevent fluorouracil-induced Nuclear Factor-κB activation in oral mucositis: in vitro and in vivo studies. *International Journal of Molecular Sciences*, **19**(10): 2981.

Toma AI, Fuller JM, Willett NJ, et al. 2021. Oral wound healing models and emerging regenerative therapies. *Translational Research*, **236**: 17–34.

Umeki H, Tokuyama R, Ide S, et al. 2014. Leptin promotes wound healing in the oral mucosa. *PLoS One*, **9**(7): e101984.

Waasdorp M, Krom BP, Bikker FJ, et al. 2021. The bigger picture: why oral mucosa heals better than skin. *Biomolecules*, **11**(8): 1165.

Wakamori S, Taguchi K, Nakayama Y, et al. 2022. Nrf2 protects against radiation-induced oral mucositis via antioxidation and keratin layer thickening. *Free Radical Biology and Medicine*, **188**: 206–220.

Wang CB, Zang K, Tang ZX, et al. 2023. Hordenine activated dermal papilla cells and promoted hair regrowth by activating Wnt signaling pathway. *Nutrients*, **15**(3): 694.

Wang LT, Fu Z, Su YH, et al. 2025. Cyclic heptapeptide FZ1 acts as an integrin αvβ3 agonist to facilitate diabetic skin wound healing by enhancing angiogenesis. *Journal of Medicinal Chemistry*, doi: 10.1021/acs.jmedchem.5c01734.

Wang XY, Yang Q, Zhou XF, et al. 2021a. Shenling Baizhu powder inhibits RV-SA11-induced inflammation and rotavirus enteritis via TLR4/MyD88/NF-κB signaling pathway. *Frontiers in Pharmacology*, **12**: 642685.

Wang Y, Feng Z, Yang MF, et al. 2021b. Discovery of a novel short peptide

with efficacy in accelerating the healing of skin wounds. *Pharmacological Research*, **163**: 105296.

Wang ZX, Liang MC, Li H, et al. 2022. L-Methionine inhibits 4-hydroxy-2-nonenal accumulation and suppresses inflammation in growing rats. *Nutrition Research and Practice*, **16**(6): 729–744.

Wu CH, Ko JL, Liao JM, et al. 2019. D-methionine alleviates cisplatin-induced mucositis by restoring the gut microbiota structure and improving intestinal inflammation. *Therapeutic Advances in Medical Oncology*, **11**: 1758835918821021.

Wu HG, Song SY, Kim YS, et al. 2009. Therapeutic effect of recombinant human epidermal growth factor (rhEGF) on mucositis in patients undergoing radiotherapy, with or without chemotherapy, for head and neck cancer: a double-blind placebo-controlled prospective phase 2 multi-institutional clinical trial. *Cancer*, **115**(16): 3699–3708.

Wu JC, Beale KK, Ma JD. 2010. Evaluation of current and upcoming therapies in oral mucositis prevention. *Future Oncology* (*London, England*), **6**(11): 1751–1770.

Wu XQ, He WJ, Mu XR, et al. 2022. Macrophage polarization in diabetic wound healing. *Burns & Trauma*, **10**: tkac051.

Wu YT, Ru ZQ, Peng Y, et al. 2024. Peptide $Cy_{RL\text{-}QN15}$ accelerates hair regeneration in diabetic mice by binding to the Frizzled-7 receptor. *Zoological Research*, **45**(6): 1287–1299.

Xie ZW, Shi JZ, Zong M, et al. 2021. Isolation and culture of primary human gingival epithelial cells using Y-27632. *Journal of Visualized Experiments*, doi: 10.3791/62978.

Yu H, Lin LB, Zhang ZQ, et al. 2020. Targeting NF-κB pathway for the therapy of diseases: mechanism and clinical study. *Signal Transduction and Targeted Therapy*, **5**(1): 209.

Zhang MF, Wan SC, Chen WB, et al. 2023a. Transcription factor *Dmrt1* triggers the SPRY1-NF-κB pathway to maintain testicular immune homeostasis and male fertility. *Zoological Research*, **44**(3): 505–521.

Zhang XY, Liang YP, Huang SF, et al. 2024. Chitosan-based self-healing hydrogel dressing for wound healing. *Advances in Colloid and Interface Science*, **332**: 103267.

Zhang Y, Wang Y, Zeng L, et al. 2022a. Amphibian-derived peptide homodimer OA-GL17d promotes skin wound regeneration through the miR-663a/TGF-β1/Smad axis. *Burns & Trauma*, **10**: tkac032.

Zhang YS, Liang XJ, Bao XF, et al. 2022b. Toll-like receptor 4 (TLR4) inhibitors: current research and prospective. *European Journal of Medicinal Chemistry*, **235**: 114291.

Zhang ZY, Zhang N, Lu XC, et al. 2023b. Anti-infection effects of heparin on SARS-CoV-2 in a diabetic mouse model. *Zoological Research*, **44**(6): 1003–1014.